Cinderella: Method Generalisation of the Elimination Process to Filter Repeating Patterns

Franz-Georg Ulmer
Remote Sensing Technology Institute
Deutsches Zentrum für Luft- und Raumfahrt (DLR)
82234 Weßling
Email: Franz-Georg.Ulmer@dlr.de

***Abstract*—Synthetic aperture radar is a popular remote sensing technique to observe the topography of the earth by producing interferograms. After initial corrections, there remains a mixture of different disturbances visible in them. Therefore, an estimation is necessary to distinguish between patterns caused by different sources. Commonly, this is achieved by using Persistent Scatterer Interferometry (PSI) or Small BAseline Subset Algorithm (SBAS) which both utilise large stacks of temporally connected interferograms of the same area. The objective of this paper is to introduce a new technique that can also handle small stacks and temporally unconnected subsets, and does not use the isotropy assumption. The introduced estimation technique, called Cinderella, is related to the elimination process and therefore belongs to the Bionic research area. The proposed technique works as follows. First, the initial images are transferred into the dual tree complex wavelet domain. Second, the Cinderella technique is applied for each complex coefficient and estimates a percentage affiliation of the corresponding wavelet to different causes. Third, the Tikhonov regularisation uses this estimate and provides the resulting assignment. Finally, the synthesis of the dual tree complex domains provides the images of all estimated signals. Verification is achieved by simulating random patterns, mixing them, applying the proposed technique, and comparing the estimates with the initial simulations. In doing so, only six interferograms were required to provide an estimation with a standard deviation below 1 mm.**

***Index Terms*—process of exclusion; Tikhonov regularisation; InSAR; atmospheric phase screen; Bionic**

I. Introduction

Synthetic aperture radar is a popular remote sensing technique to observe the topography of the earth. Differential interferometric synthetic aperture radar (**DInSAR**) images are subtracted phase information of two synthetic aperture radar acquisitions (master - slave acquisition scene). Observed signals within a DInSAR result from a deformation of the topography, atmospheric and ionospheric conditions, errors of the used digital elevation model, and noise (see [1]).

If the topographic deformation is the purpose of the monitoring, all disturbing signals have to be compensated. Different preprocessing steps reduce the errors, but some residual errors are still present within a single interferogram. Therefore, stacks of DInSAR images of the same area are utilised to filter the desired signal from the disturbances. For example, the temporal linear deformation (centre image in Figure 1) is included in every interferogram (surrounding images) and forms the stack. Each interferogram is in the same way affected by the atmosphere of the master and changing atmosphere of the slave scenes in this example. These disturbances are filtered from the stack, such that just the deformation remains (see Figure 3, right column). Common assumptions are that the disturbances are uncorrelated and that the desired signal is correlated with time (see [1]). Unfortunately, this technique fails if the size of the stack is too small, i.e. errors are still too large.

Generally, a regression analysis estimates the desired signals (x) from the observed interferograms y by (utilisation for PSI, see [2])

$$\text{argmin}_x ||Ax - y||_2^2 \tag{1}$$

where matrix A describes the linear relationship between the unobservable vector x and observations y (see [6]).

Practically, this technique is sensitive to outliers and has required large stacks up to the present time. The necessary stack size is reduced by knowing these outliers and weighting the corresponding observations less heavily. Often, it is helpful to identify visually the faulty interferograms that have strong disturbances, and to ignore them. Naturally, the eye looks for repeating patterns at the same location in different DInSAR images. Here, a pattern signifies that the pattern is well approximated by just a few wavelets and is not necessarily isotropic. Those interferograms, inheriting many changing patterns are identified as outliers. This intuitive approach by inspection of the data is time-consuming, and repeating signals may be misinterpreted. For example, digital elevation model errors often occur also at the same location like it is expected for deformations. Therefore, a technique is needed that automatically identifies repeating patterns and assigns them to their most plausible cause. The natural process of visually inspecting the data is binary, i.e. each pattern belongs exclusively to one cause and may fail at special conditions. Hence, this needed technique should also generalise this binary assignment to percentage assignment.

The dual tree complex wavelet transform ($DT\mathbb{C}WT$) represents images in a sparse way, and the framework can be found in [3], [4]. In such a transform, a pattern is concentrated in a

few complex-valued coefficients, allowing the identification of repeating patterns by looking for repeated large coefficients. Therefore, the introduced technique is applied within the $DT\mathbb{C}WT$ domain.
Different causes contribute to different interferograms in varying magnitude. For example, a temporal linear deformation in time is characterised by the temporal distance (temporal baseline) between the acquisition times of an interferogram. Therefore, if the temporal baselines of two interferograms are related by a factor, the deformation signals are also related by this factor. Hence, a linear combination of all interferograms can be built, such that the pattern that is being sought must vanish. Every pattern that is still present, cannot be the desired pattern and does not belong to the desired cause. This elimination process is generalised (denoted by Cinderella), allowing the estimation of the inverse covariance matrix (C^{-1}) of x. The Tikhonov regularisation ($||x||^2_{C^{-1}}$) is utilised to extend equation 1 to

$$\text{argmin}_x ||Ax - y||_2^2 + ||x||^2_{C^{-1}} \tag{2}$$

where $||x||^2_{C^{-1}}$ is the weighted norm $xC^{-1}x$ (see [5], [6]). This allows us to find repeating patterns by using the $DT\mathbb{C}WT$, estimating the percentage affiliation by estimating C^{-1} and assigning them by solving the equation 2.

The objective of this work is the methodical introduction of the proposed technique and its validation. Accordingly, linear deformation estimations of the proposed technique and the stacking technique are compared against each other.

II. Methods

First, the initial interferograms are unwrapped and corrected to the greatest extent possible. Second, the coarsely-corrected interferograms are transferred into the complex-valued wavelet domain by utilising the $DT\mathbb{C}WT$. Third, for each complex coefficient within the wavelet domain, the Cinderella algorithm is applied, and thereby the percentage affiliation is estimated and assigned by the equation 2. Finally, the synthesis (inverse transform of the $DT\mathbb{C}WT$) provides the final estimated causes as images.

For the generalisation, the shape of A is linked to the exclusion principle, and its detailed shape is derived in the following paragraph. Starting with the nomenclature, the X_i will denote different kinds of processes, such as atmospheric phase screens (**APS**), deformations that depend on temporal linear properties, or digital elevation model (**DEM**) errors depending on the baseline or other processes. For motivation, consider two DInSARs with equidistant temporal baselines and the same master scene. For simplicity, it is assumed that the disturbances only correspond to the APSs. Now, the signals are separated from the atmospheric phase screens (X_1, X_2, X_3) of the three different acquisitions from the deformation, which are temporally dependent (X_4). The interferograms are mathematically described by

$$Y_1' = X_2 - X_3 - X_4 \tag{3}$$

$$Y_2' = X_2 - X_1 + X_4 \tag{4}$$

where the master scene is the second acquisition with APS X_2. The slave scene APSs are therefore X_1 and X_3. The deformation X_4 has the opposite direction ($+/-X_4$) within the interferograms Y_1' and Y_2', because the temporal distance has alternate signs. The corresponding linear equation system is under-determined and is expressed by the matrix

$$\mathbf{A}' := \begin{pmatrix} 0 & 1 & -1 & -1 \\ -1 & 1 & 0 & 1 \end{pmatrix} \begin{matrix} \text{(I)} \\ \text{(II)} \end{matrix}$$

where $\mathbf{A}'\boldsymbol{X} = \boldsymbol{Y}'$, $\boldsymbol{X}^{\mathrm{T}} = (X_1, X_2, X_3, X_4)$ and $\boldsymbol{Y}'^{\mathrm{T}} = (Y_1', Y_2')$. By adding, subtracting and reordering the rows of $\mathbf{A}'$, we find

$$\mathbf{A} := \begin{pmatrix} 0 & 1 & -1 & -1 \\ -1 & 0 & 1 & 2 \\ -1 & 1 & 0 & 1 \\ -1 & 2 & -1 & 0 \end{pmatrix} \begin{matrix} \text{(I)} \\ \text{(II} - \text{I)} \\ \text{(II)} \\ \text{(I} + \text{II)} \end{matrix},$$

$\boldsymbol{Y}^{\mathrm{T}} = (Y_1', Y_2' - Y_1', Y_2', Y_1' + Y_2')$ such that $\mathbf{A}\boldsymbol{X} = \boldsymbol{Y}$.

Matrix $\mathbf{A}$ has zeros on the diagonal, and on the off-diagonal, it has only nonzero values. Assume that in Y_1, Y_2 and Y_3, the same pattern is always visible, but missing in Y_4. Now, the exclusion principle states that this pattern is caused by the deformation, because it is the only process at the fourth row of A that is not present (has 0 value). Therefore, the shape of A provides the utilisation of the exclusion principle.
The following generalises this approach by transforming the linear equation problem into an estimation problem. Therefore, the variances of the X_i are model parameters (σ_i^2) that will be estimated. First, an assumed model parametrisation of the X_i (σ_i^2) implies variances of the Y_i ($\tilde{\mathrm{V}}\,\boldsymbol{Y}_i$). Second, the observations of the complex coefficients provide the sample variances ($\hat{V}\boldsymbol{Y}_i$). Third, the sample variance and the implicit variance are compared against each other. If they do not match well, the assumed model parametrisation (σ_i^2) was wrong. Now, these model parameters (σ_i^2) are selected such that all differences ($|\,\tilde{\mathrm{V}}\,\boldsymbol{Y}_i - \hat{V}\boldsymbol{Y}_i|$) are minimal. For improved readability, the problem is rewritten and generalised for higher dimensions. It is assumed that every stochastic process $X_i \sim \mathcal{N}(0, \sigma_i)$ where the model parameter $\mathrm{V}\boldsymbol{X} = (\sigma_1^2, \ldots, \sigma_n^2) \in \Theta$ are estimated. Later, they form C^{-1} in the equation 2. Remember, the X_i are not observable, but rather linear combinations of them are observed. From now on, $\boldsymbol{X}^T = (X_1, \ldots, X_{\mathrm{n}})$ and the observable random variable $\boldsymbol{Y}^T = (Y_1, \ldots, Y_{\mathrm{n}})$ are related by the following equation:

$$\mathbf{A}\boldsymbol{X} = \boldsymbol{Y}. \tag{5}$$

$\mathbf{A}$ is constructed as in the previous example, such that $\mathbf{A} \in \mathbb{R}^{\mathrm{n}\times\mathrm{n}}$, $\mathbf{A}_{i,i} = 0$ for all $i \in \{1, ..., \mathrm{n}\}$ and $\mathbf{A}_{i,j} \neq 0$ for $i \neq j$. Each parametrisation $\mathrm{V}\boldsymbol{X} \in \Theta$ implies the variances of the $\boldsymbol{Y}_i$ by the formula of Bienaymé. Remember, $\mathrm{V}\boldsymbol{X}$ is not known and therefore neither is the real variance of $\boldsymbol{Y}$. Because of

this, we denote and compute the implicit variance by

$$\tilde{\mathrm{V}}\,\boldsymbol{Y}_i = \sum_{k=1}^{n} \mathbf{A}_{k,i}^2 \sigma_k^2. \tag{6}$$

The randomly-observed sample variance $\hat{V}\boldsymbol{Y}_i$ of m independent observations is defined as a random variable. The Y_i are centred, because the X_i are centred, such that

$$\hat{V}\boldsymbol{Y}_i = \frac{1}{m}\sum_{k}^{m} \boldsymbol{Y}_{ik}^2. \tag{7}$$

It is expected that $\hat{V}\boldsymbol{Y}_i \approx \mathrm{V}\,\boldsymbol{Y}_i = \tilde{\mathrm{V}}\,\boldsymbol{Y}_i$ if for each $k \in \{1,\ldots,n\}$ the model parameter σ_k^2 equals the true variance of X_k ($\mathrm{V}\,X_k$). Now, these model parameters are chosen such that all observed differences ($\hat{V}\boldsymbol{Y}_i - \tilde{\mathrm{V}}\,\boldsymbol{Y}_i$) are minimal, exactly as expected.

In order to normalise the difference it is divided by $\tilde{\mathrm{V}}\,\boldsymbol{Y}_i$. Thus,

$$T_i = |\frac{\hat{V}\boldsymbol{Y}_i}{\tilde{\mathrm{V}}\,\boldsymbol{Y}_i} - 1|. \tag{8}$$

Due to the normalisation, all T_i have the same distribution such that a balanced situation is established. Let t_i be an observation of T_i, then

$$v = \mathrm{argmin}_{(\sigma_1^2,\ldots,\sigma_n^2)} |(t_1,\ldots,t_n)|_2^2 \tag{9}$$

is computed. For the demonstration at the end of this work, the minimisation was computed by the Powell algorithm (see [7]).

Because of the independence of the X_i, the diagonal inverse covariance matrix from the equation 2 is $C_{i,i}^{-1} = v_i^{-1}$. Then, the solution of equation 2 provides the percentage assignment of the complex coefficient and the related wavelet. Finally, for all processes X_i, the synthesis (inverse dual tree complex wavelet transform) provides the final estimates of the independent causes.

III. Results

First, the relationship of the proposed technique to the exclusion principle is illustrated by an example. Then, the solutions of the exclusion principle and the introduced technique are compared. Next, a validation is provided by simulating random patterns (ground truth), mixing them (input data), separating them by the proposed technique, and comparing them with the ground truth that was initially established.

A. Relationship of the Cinderella approach to the exclusion principle

Remember, the motivation of the presented algorithm is the relationship of it to the exclusion principle. To provide an example, this relationship is briefly illustrated. Let

$$A = \begin{pmatrix} 0 & 1 & 1 \\ 1 & 0 & 1 \\ 1 & -1 & 0 \end{pmatrix}, y = \begin{pmatrix} 1 \\ 1 \\ \epsilon \end{pmatrix} \tag{10}$$

then $Ax = y$ is ill-posed. Now, if $\epsilon = 0$, then the exclusion principle provides a reasonable solution $x^T = (0,0,1)$, because at the third row of A, only the third entry vanished as well as the third observation y_3. This argumentation is false if $\epsilon \neq 0$, but the presented method provides a solution. It is

$$v = (\frac{\epsilon^2}{2}, \frac{\epsilon^2}{2}, 1 - \frac{\epsilon^2}{2})^{\mathrm{T}} \tag{11}$$

because for all $i \in \{1,2,3\}$, the sample variance

$$\hat{V}\boldsymbol{Y}_i = y_i^2 \tag{12}$$

equals the implicit variance

$$\tilde{\mathrm{V}}\,\boldsymbol{Y}_i = A_{i,1}^2 v_1 + A_{i,2}^2 v_2 + A_{i,3}^2 v_3, \tag{13}$$

and therefore, $t_i = 0$ thus $t_1 + t_2 + t_3 = 0$ is minimal. So, v converges against the solution of the exclusion principle if $\epsilon \to 0$.

B. Validation with synthetic data

The validation is provided in four steps. First, synthetic data are simulated for a typical deformation as well as textured atmospheric disturbances. Typically, a subsidence or uplift causes a Gaussian bell-shaped pattern while the atmosphere is more chaotic. Patterns that are caused by, for example, cold fronts, topographically-related eddies, or gravity waves have different spatial dependencies at different locations (refer to examples provided in [8]). Therefore, a sinus with different offsets and frequencies generates the initial simulated APS. Further, the APS is multiplied by simulated fractal noise using a Hurst parameter of $H = 0.7$ to render it realistically. A rescaled-range analysis (see [9]) of Global Navigation Satellite System (**GNSS**) zenith time-delay series at Kokkee Park in Hawaii and Wetzell in Germany has confirmed this parameter setting. Typically, the standard deviations of the residual APSs are approximately 15mm (see GNSS–ECMWF in [10]), and the simulated linear deformation has a velocity of 10mm/12days. Together, 10 simulated processes x_i are derived, where the first 9 correspond to the APS, and the final one to the deformation.

Second, eight synthetic interferograms ($i \in \{1,\ldots,8\}$)

$$y_i = x_1 - x_{i+1} + i x_{10} \tag{14}$$

are simulated and form the test data set (see Figure 1). Third, on subsets of the test data set, the introduced technique and the stacking technique are applied, providing two different kinds of estimates of the linear deformation (see Figure 3). Fourth, the standard deviations of the residual disturbances (estimates – ground truth) are computed and compared against each other (see Figure 2).

Therefore, six subsets of the initial images are

$$S_i = \{y_1,\ldots,y_{i+2}\}, \tag{15}$$

providing six pairs of standard deviation. The introduced technique compensates the APS to a greater extent and converges against the true deformation if the stack size increases. This is visible from top to bottom in the right column of Figure 3. In comparison, the estimation of the stacking technique (left column) does not remove the APS. Consequently, the

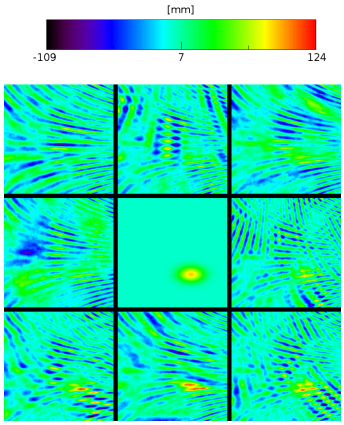

Fig. 1. The centre image shows the synthetic deformation in the strongest occurrence within a synthetic interferogram (lower right). Synthetic interferograms are displayed from left to right, and from top to bottom.

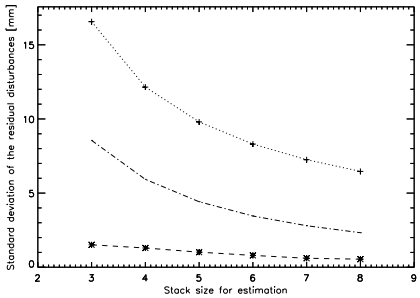

Fig. 2. The graph shows the standard deviation of the residual disturbances (estimate – ground truth deformation) of the stacking technique ($+$) and the Cinderella technique ($*$). Additionally, the middle function ($-\cdot-$) corresponds to the analytical accuracy of the PSI technique.

standard deviations in Figure 2 converge quickly towards 0 for the Cinderella estimates in contrast, this is not true for the stacking technique estimates.

IV. Discussion

Now, the proposed technique is compared against the commonly used PSI technique. Remember, the PSI technique is based on frequency estimation (i.e. no phase unwrapping) whereas Cinderella adds a regularisation term which is estimated in a first step. Accordingly, the Cinderella algorithm is more computational time consuming and requires a phase unwrapping. On the other hand, for PSI the accuracy of the linear deformation estimate is given by

$$\sigma_d = \sigma_a \sqrt{\frac{1}{N \mathrm{Var}(X_d)}} \tag{16}$$

where $\sigma_a \approx 21$mm is the atmospheric distortion, N is the number of interferograms and $\mathrm{Var}(X_d)$ is the variance of the deformation in utilised interferograms. Corresponding function is plotted in figure 2 drawn with $- \cdot -$. Consequently, 16 interferograms are required to reach an accuracy of 1mm. In comparison, Cinderella needs only 6 interferograms, illustrating practical advantage.

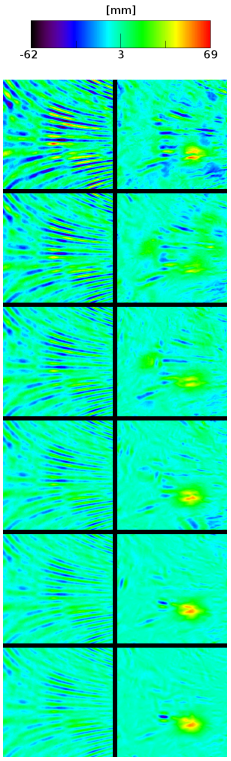

Fig. 3. The left column displays the stacking technique estimation for the linear deformation within a month. The right column displays the estimates of the Cinderella approach of the linear deformation for six months. Different time scales are necessary to see the deformation within the Cinderella technique because of its strong noise reduction.

Two new challenges arise. First, the minimisation 9 is done by the Powel algorithm (see [7]) and is therefore computational time consuming. Accordingly, a faster algorithm to derive the global minimum is needed. Second, from a statistical point of view, the T_i are treated as independent observations for simplicity. Therefore, a potential further development is achieved by introducing a decorrelation step for the T_i. Consequently, a higher accuracy should be derived.
Naturally, Cinderella is adoptable for other problems which are related to the linear regression analysis. However, the most advantage of Cinderella in comparison to the straight forward linear regression analysis is achieved in sparse domains. This is the case, because Cinderella is closely related to the exclusion principle.

V. Conclusion

The introduced technique filters signals from a stack of interferograms that correlate more closely with a predefined relationship between the interferograms. Therefore, the proposed technique filters undesired signals and provides a better estimate of the desired signal in comparison with the stacking technique and PSI. If the stack size is too small, such that PSI and SBAS are not applicable, the introduced technique still has the ability to filter signals even if the subsets of interferograms are temporarily not connected.

ACKNOWLEDGMENT

The author would thank Nicole Richter, Christian Minet, Moritz Fischer, Nico Adam and Malte Rosenthal for their proofreading, comments and discussions. Thanks also to Nick Kingsbury, who provided Q-shift filters for the $DT\mathbb{C}WT$.
I thank E-GVAP, the E-GVAP processing centres, and the GNSS data-owners for access to the E-GVAP NRT GNSS delay data (http://egvap.dmi.dk). Thanks to the International GNSS Service (IGS), which also provided delay data (http://igscb.jpl.nasa.gov).

REFERENCES

[1] B. Kampes, *Radar interferometry: persistent scatterer technique*, ser. Remote sensing and digital image processing. Springer, 2006.

[2] A. Ferretti, C. Prati, and F. Rocca, "Permanent scatterers in SAR interferometry," *Geoscience and Remote Sensing, IEEE Transactions on*, vol. 39, no. 1, pp. 8–20, 2001.

[3] I. W. Selesnick, "The design of approximate Hilbert transform pairs of wavelet bases," *Signal Processing, IEEE Transactions on [see also Acoustics, Speech, and Signal Processing, IEEE Transactions on]*, vol. 50, no. 5, pp. 1144–1152, 2002. [Online]. Available: http://ieeexplore.ieee.org/xpls/abs_all.jsp?arnumber=995070

[4] I. Selesnick, R. Baraniuk, and N. Kingsbury, "The dual-tree complex wavelet transform," *Signal Processing Magazine, IEEE*, vol. 22, no. 6, pp. 123 – 151, nov. 2005.

[5] A. Tikhonov and V. Arsenin, *Solutions of ill-posed problems*, ser. Scripta series in mathematics. Winston, 1977. [Online]. Available: http://books.google.co.in/books?id=ECrvAAAAMAAJ

[6] A. Björck, *Numerical Methods for Least Squares Problems*. Society for Industrial and Applied Mathematics, 1996. [Online]. Available: http://books.google.de/books?id=myzIPBwyBbcC

[7] M. J. D. Powell, "An efficient method for finding the minimum of a function of several variables without calculating derivatives," *The Computer Journal*, vol. 7, no. 2, pp. 155–162, Jan. 1964. [Online]. Available: http://dx.doi.org/10.1093/comjnl/7.2.155

[8] R. F. Hanssen, T. M. Weckwerth, H. A. Zebker, and R. Klees, "High-resolution water vapor mapping from interferometric radar measurements," *Science*, vol. 283, no. 5406, pp. 1297–1299, 1999.

[9] R. M. Bryce and K. B. Sprague, "Revisiting detrended fluctuation analysis." *Scientific reports*, vol. 2, 2012. [Online]. Available: http://view.ncbi.nlm.nih.gov/pubmed/22419991

[10] K. Teke, T. Nilsson, J. Böhm, T. Hobiger, P. Steigenberger, S. García-Espada, R. Haas, and P. Willis, "Troposphere delays from space geodetic techniques, water vapor radiometers, and numerical weather models over a series of continuous VLBI campaigns," *Journal of Geodesy*, vol. 87, no. 10-12, pp. 981–1001, 2013. [Online]. Available: http://dx.doi.org/10.1007/s00190-013-0662-z